1

2

3

4

5 **RecA levels modulate biofilm development in *Acinetobacter baumannii***

6 Carly Ching[1,2], Paul Muller[1], Merlin Brychcy[1], Alicyn Reverdy[1], Brian Nguyen[1], Margaret Downs[1,3],

7 Samuel Regan[4], Breanna Isley[1], William Fowle[1], Yunrong Chai[1], and Veronica G. Godoy[1*]

8

9 [1]Northeastern University, Department of Biology, Boston, MA, 02115

10 [2]Current address: Department of Biomedical Engineering, Boston University, Boston, MA, 02215

11 [3]Current address: Department of Biochemistry, Boston University School of Medicine, Boston, MA

12 02118.

13 [4]Current Address: Transitional Year Resident at St. Joseph Mercy Ann Arbor, 5301 McAuley Dr.,

14 Ypsilanti, Michigan 48197.

15

16

17

18

19 * Corresponding Author: Veronica G. Godoy, v.godoycarter@northeastern.edu

20

Abstract

Infections caused by *Acinetobacter baumannii,* a Gram-negative opportunistic pathogen, are difficult to eradicate due to the bacterium's propensity to quickly gain antibiotic resistances and form protective bacterial multicellular communities known as biofilms. The *A. baumannii* DNA damage response (DDR) mediates antibiotic resistance acquisition and regulates RecA in an atypical fashion; both $RecA^{Low}$ and $RecA^{High}$ cell types are formed in response to DNA damage. In this study, we show that RecA levels modulate biofilm development, formation and dispersal, through *bfmR*, the global biofilm regulator. RecA loss results in surface attachment and prominent biofilms while elevated RecA leads to diminished attachment and dispersal. Recalcitrance to treatment may be explained by DDR induction, common during infection, and the balance between biofilm maintenance in low RecA cells, and increased mutagenesis and dispersal to reach new niches in high RecA cells. These data highlight the importance of understanding fundamental biology to better treat bacterial infections.

Impact

The mechanism of biofilm formation and dispersal in *A. baumannii*, shown here to depend on RecA levels, contributes to the understanding of recalcitrant infections caused by this important pathogen.

42 **Introduction**

43 *Acinetobacter baumannii* is an emerging Gram-negative opportunistic pathogen and one of the
44 ESKAPE pathogens, a group of bacteria responsible for most hospital-acquired infections (Rice, 2008).
45 *A. baumannii* outbreaks in hospitals are difficult to eradicate, due to increased multi-drug resistance
46 (MDR) (Peleg et al., 2008) and its ability to form biofilms (Eze et al., 2018). *A. baumannii* infections
47 are very dangerous to immunocompromised individuals, causing various illnesses, including
48 pneumonia, septicemia, and wound infections (Smith et al., 2007).

49

50 When gene products involved in antibiotic binding or processing on the chromosome are mutated,
51 resistance is acquired (Blair et al., 2014). One response pathway underlying multidrug resistance
52 (MDR) is the DNA damage response (DDR). Mutagenesis results from induction of error-prone DNA
53 polymerase genes which are part of the DDR regulon (Cirz et al., 2007; Fuchs and Fujii, 2013). We
54 have shown that in *A. baumannii*, RecA-dependent induction of multiple error-prone polymerases in
55 response to DNA damage leads to clinically relevant antibiotic resistance (Norton et al., 2013). In
56 *Escherichia coli* and many other bacteria, the cells' main recombinase, RecA, and the global
57 transcriptional repressor, LexA, manage the DDR, also known as the SOS response (Little and Mount,
58 1982). In contrast, there is no known LexA homologue in *A. baumannii*, indicating the *A. baumannii*
59 DDR circuitry is regulated differently (Ching et al., 2017; Hare et al., 2014; MacGuire et al., 2014;
60 Norton et al., 2013). We also showed that in response to DNA damage there are two RecA cell types,
61 low *recA* expression ($RecA^{Low}$) and high *recA* expression ($RecA^{High)}$, regulated by a 5'untranslated
62 region in the *recA* transcript(Ching et al., 2017; MacGuire et al., 2014).

63

64 Bacterial cells within biofilms are often less sensitive to chemical and physical challenges, including
65 antibiotics (Anderl and Franklin, 2000; Singh et al., 2016). Like many biological processes, the biofilm
66 cycle in *A. baumannii* is not fully understood, though key biofilm genes have been described, including
67 the biofilm master regulator gene *bfmR* that controls adhesive *csu* pili and genes important for virulence
68 and desiccation tolerance (Farrow et al., 2018; Tomaras et al., 2008, 2003). It is also known that genes
69 encoding Bap protein and efflux pumps are important for biofilms (Brossard and Campagnari, 2012;
70 He et al., 2015; Loehfelm et al., 2008; Tomaras et al., 2008, 2003). The BfmR response regulator is
71 part of a two-component system (BfmRS) (Farrow et al., 2018; Geisinger and Isberg, 2015; Russo et
72 al., 2016; Tomaras et al., 2008; Wang et al., 2014) that results in BfmR phosphorylation. It is unknown
73 if *bfmR* expression is induced by another factor or whether de-repression by phosphorylated BfmR,
74 with lower affinity for its operator site (Draughn et al., 2018), is enough for induction. The *A.*
75 *baumannii* biofilm extracellular matrix has been reported to contain poly-ß-(1-6)-*N*-acetyl-
76 glucosamine, mannose and extracellular DNA (Bales et al., 2013; Choi et al., 2009; Hardouin et al.,
77 2014; Sahu et al., 2012).

78

79 In summary, the DDR and the biofilm cycle are two developmental pathways in bacteria to assure
80 genomic stability and survival. In some bacteria, antibiotics and DNA damaging agents have been
81 observed to induce biofilm formation, suggesting a link between these two pathways (Linares et al.,
82 2006; Takajashi et al., 1995). However, the mechanisms linking the DDR and biofilms varies between
83 bacterial species. For example, in *Streptococcus mutans*, *Escherichia coli* (Costa et al., 2014; Inagaki
84 et al., 2009), and *Clostridium difficile* (Walter et al., 2015) there is a direct correlation between DDR
85 and biofilms in which both pathways are induced in response to environmental signals. However, we
86 showed that during *Bacillus subtilis* biofilm development, induction of the DDR shuts off biofilm
87 matrix genes in a subpopulation of cells (Gozzi et al., 2017), indicating an inverse correlation between

88 DDR and biofilm formation. In this case, DDR signaling complements the biofilm cycle, and cells that
89 are DDR-induced could potentially leave the biofilm to search for new niches. Altogether, the varied
90 relationships between DDR and the biofilm cycle are intriguing and show that cells have evolved
91 different ways to balance these strategies, which could have downstream effects in treatment and
92 clinical practices.

93

94 Here, we demonstrate that the DDR and the biofilm cycle intersect in *A. baumannii*. We show that loss
95 of RecA in *A. baumannii* results in increased cell-to-surface adherence, in part due to elevated
96 expression of *bfmR* with a concomitant increase in Csu pili. We further identify novel regulation of
97 *bfmR* through the RecA-dependent UmuDAb gene product. We observed that DNA damaged biofilm
98 pellicles shut off *csuAB* gene expression, turn on *recA*, and cells disperse. The observed inverse
99 relationship between DDR and biofilm formation may lead to a heterogeneous population combining
100 physical (biofilm) and genetic (elevated mutagenesis) protection to environmental challenges.

101

102 **Results**

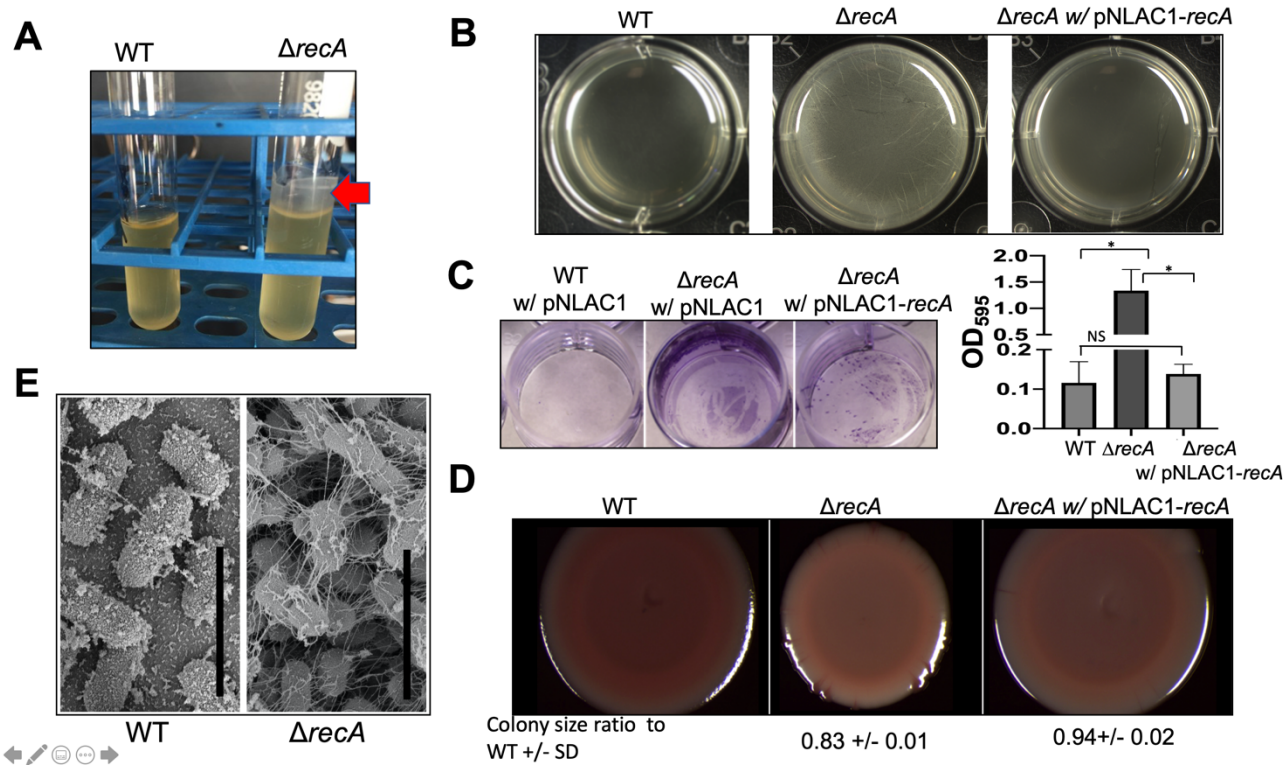

Figure 1. RecA negatively influences surface attachment and biofilm formation. (A) Saturated Δ*recA* cell cultures show growth on the side surface of glass test tubes (red arrow) compared to WT cells. **(B)** Δ*recA* forms visible pellicles biofilms at the air-liquid interface earlier than its isogenic WT counterpart. Biofilm pellicles of WT (with empty PNLAC1 plasmid), Δ*recA* (with empty PNLAC1 plasmid), and the complemented strain (Δ*recA*(pNLAC1-*recA*)) at 24 hrs. Representative images are shown. **(C)** Δ*recA* cells adhere to the abiotic surface better than WT and the Δ*recA* complemented strain (Δ*recA*(pNLAC1-*recA*)). Left panel displays wells after Crystal Violet staining. Right panel shows absorbance at 595 nm for Crystal Violet staining of polystyrene surface-adhered cells at 24 hrs. Experiments were performed in triplicate and error bars shown represent standard deviation of the mean. An unpaired two-tailed T-test was performed for statistical analysis, * =P < 0.05. Brackets above the columns show the comparisons made. NS=not significant **(D)** RecA influences colony biofilm architecture and coloration. Differences in Congo Red coloration is an indication of biofilm matrix alterations. Colony biofilms of WT, Δ*recA* and complemented Δ*recA* strains on plates at 48 hrs. Numbers shown underneath the images represent the average diameter of 3 colonies from images taken at the same magnification and settings in 3 independent experiments relative to the WT colony diameter set as 1. The error shown is the standard deviation of the mean. **(E)** Δ*recA* biofilms have increased observable matrix compared to WT biofilms. Scanning electron microscopy (SEM) of WT and Δ*recA* biofilms collected on coverslips at 24 hrs. Scale bar is 3μm.

103

104

105 **Loss of RecA promotes biofilms in *A. baumannii***

106 *A. baumannii* ATCC 17978 Δ*recA* cells (*recA*::km, Table S1 (Aranda et al., 2011)) grown in standard
107 LB medium and shaking conditions consistently displayed observable surface attachment on the sides
108 of glass tubes (Fig. 1A, red arrow). In comparison, the parental wild-type strain had little to no surface
109 attachment (Fig. 1A). This observation suggested that *A. baumannii* Δ*recA* cells form more biofilm
110 than WT cells. Since lack of RecA can presumably affect bacterial growth (Cox et al., 2008), we
111 performed growth measurements of free-living planktonic WT and Δ*recA* cells. We also measured
112 growth in Δ*recA* cells complemented with a low-copy plasmid, pNLAC1(Luke et al., 2010), containing
113 *recA* under its own promoter (Ching et al., 2017) (Δ*rec*A (pNLAC1-*recA*), Table S1), which we will
114 refer to as the complemented Δ*recA* mutant. We observed a slight growth disadvantage in Δ*recA* cells
115 whenever the starting inoculum size was $<10^7$ cells that was rescued by the extrachromosomal copy of
116 *recA* (Fig S1A & B). Our result is largely consistent with a previous report that the Δ*recA* strain showed
117 no noticeable growth defects compared to the parental WT strain (Aranda et al., 2011).

118

119 To further assay biofilm formation, we prepared pellicle biofilms (formed at the air-liquid interface)
120 with Δ*recA* and WT cells as indicated in materials and methods. WT cells did not form a visible pellicle
121 (Fig. 1B, left) at 24 hrs while Δ*recA* cells (Fig. 1B, middle) formed a visible and opaque pellicle as
122 early as 24 hrs, consistent with previous observations (Fig. 1A). At 48 and 72 hrs the WT cells formed
123 a pellicle that was smooth and with striations while the Δ*recA* pellicle was thicker and granular on the
124 surface (Fig. S2). Cell adherence to the sides/bottom of the wells were measured by Crystal Violet
125 staining. We observed a significant increase in surface-attached cells in Δ*recA* biofilms at 24 hrs
126 compared to WT cells (Fig. 1C). These data suggest that Δ*recA* makes prominent biofilms compared
127 to the WT strain. To confirm that the observed Δ*recA* biofilms are indeed due to loss of RecA, we
128 tested the Δ*recA* complemented strain for biofilm formation. At 24 hrs, there was less observable

129 pellicle formation in the complemented strain (Fig 1B, right), and surface architecture was similar to
130 WT (Fig. S2).

131

132 Biofilm formation is also studied at the colony level (growth at the air-surface interface) (Vlamakis et
133 al., 2013). Typically, robust colony biofilms have more wrinkling surface architecture due to
134 differential cell death and mechanical forces as a result of increased extracellular matrix (Asally et al.,
135 2012). Thus, we grew colony biofilms on solid medium plates containing Congo red and Coomassie
136 brilliant blue, dyes that detect changes in biofilm matrix components (Ghodke et al., 2019; Surgalla
137 and Beesley, 1969). At 48 hrs, the Δ*recA* colony biofilm had differential coloring to the WT and
138 complemented strain indicative of increased biofilm matrix production (Fig 1D). We noticed that the
139 Δ*recA* colony biofilms also had decreased diameter size throughout the length of the experiment.
140 Notably, the complemented Δ*recA* colony is similar in size to WT but with an intermediate coloration
141 (Fig. 1D). We have previously observed partial complementation of colony biofilms phenotypes with
142 plasmid borne ectopic gene copies, possibly due to the sensitivity of the process to gene dosage (Ching
143 et al., 2018). The data obtained from these experiments suggest that the Δ*recA* strain forms robust
144 biofilms.

145

146 **Inverse relationship between RecA and biofilm is not exclusive to *A. baumannii* ATCC 17978**

147 To assess whether this finding was exclusive to *A. baumannii* ATCC 17978, we used a transposon
148 derivative of *A. baumannii* AB5075 in which the transposon is inserted approximately in the middle of
149 the RecA ORF (Gallagher et al., 2015) (Table S1). *A. baumannii* AB5075 is a highly virulent clinical
150 isolate (Jacobs et al., 2014). For pellicle biofilms at 48 hrs, the AB5075 insertional *recA::Tn* mutant
151 had significantly increased cell adherence compared to the parental strain (Fig. S3A). Furthermore, the

152 AB5075 *recA::Tn* mutant colony biofilm is also smaller than the parental strain and displays
153 differences in colony morphology, including changes in opacity and striations on the edge (Fig. S3B).
154 These data suggest that the observation that RecA negatively impacts biofilm development is not
155 exclusive to the ATCC 17978 strain.

156 **RecA modulates the biofilm matrix in *A. baumannii***

157 Since Δ*recA* forms prominent biofilms, we were curious to observe closely the differences between
158 Δ*recA* and WT biofilms, especially regarding the extracellular matrix. Thus, we analyzed Δ*recA* and
159 WT pellicle biofilms by scanning electron microscopy (SEM). To observe pellicle biofilms from the
160 WT and Δ*recA* strains we used a fixing procedure that takes advantage of cationic dyes binding to
161 negatively charged polysaccharides and preserve these for imaging (Erlandsen et al., 2004). We found
162 that there were noticeable differences between the matrix and biofilm structures of the WT and Δ*recA*
163 strains (Fig. 1E). At 24 hrs WT cells have some matrix and connection between cells, while Δ*recA*
164 cells were embedded in an observable thick matrix (Fig. 1E). This finding suggests that Δ*recA* cells
165 produce extracellular matrix earlier in their biofilm development.

166

167 **Surface-attached cells withstand antibiotic treatment**

168 Biofilms have been noted to protect bacteria from antibiotic exposure (Anderl and Franklin, 2000;
169 Singh et al., 2016). To determine if there were any differences in antibiotic susceptibility of the WT
170 and Δ*recA* biofilms compared to free-living cells, surface-attached WT and Δ*recA* biofilms were
171 treated with the bactericidal aminoglycoside gentamicin. First, we determined the MIC of gentamicin
172 for exponentially growing free living planktonic cells and found it to be the same for both WT and
173 Δ*recA* cells (1.88 μg/mL, error within 2-fold). Aranda *et al*. determined the MIC in free living

174 planktonic cells to Amikacin and Tobramycin, both aminoglycosides, and reported that these were also
175 the same for the WT and Δ*recA* strains (1.5 µg/mL and 0.38 µg/mL, respectively) (Aranda et al., 2011).

176

177 To assess whether biofilms withstand gentamicin treatment differently to planktonic cells, the spent
178 growth medium from 72 hr pellicle biofilms was removed, the wells were washed to eliminate non-
179 attached cells and gentamicin was added in fresh growth medium at different concentrations, and wells
180 were incubated for 24 hrs. After exposure to gentamicin, the growth medium and non-attached cells
181 were removed, and Crystal Violet staining was performed as before. Strikingly, there were more
182 surface-attached Δ*recA* cells suggesting that they withstood treatment better than WT cells (Fig. 2A).
183 For the Δ*recA* strain, the percentage of surface-attached cells remaining after antibiotic treatment
184 plateaus above 50% relative to no treatment after exposure to 0.47–15 µg/mL of gentamicin (Fig. 2B),
185 representing over 3-fold excess of Δ*recA* surface-attached cells compared to WT (at 15 µg/mL the
186 percentage of WT surface-attached cells decreases to ~16% relative to no treatment).

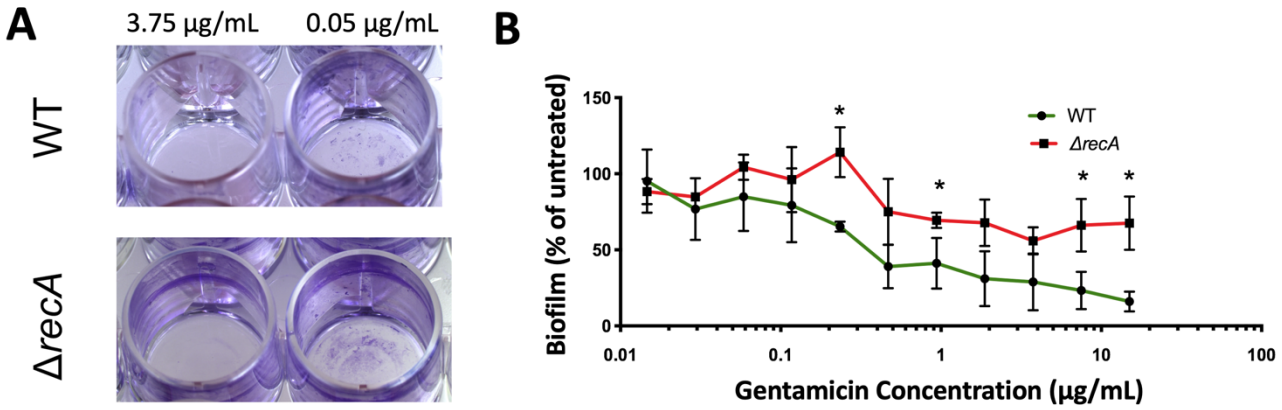

Figure 2. Biofilm formation influences antibiotic challenge (A) The Δ*recA* strain forms stronger biofilms and withstands gentamicin treatment better than the WT. Images of Crystal Violet staining representing cell attachment of 72 hr mature biofilms formed by Δ*recA* and WT after 24 hrs of gentamicin treatment. The concentrations shown are those below and above the MIC measured for free-living planktonic cells. **(B)** Percentage eradication of biofilms (A595 of exposed biofilm/A595 of untreated parental biofilm) treated with a range of gentamicin concentrations for WT and Δ*recA* cells. Experiments were performed in triplicate. Error bars represent standard deviation. An unpaired two-tailed T-test was performed to compare percentage of eradication between WT and Δ*recA* cells for each antibiotic concentration, * = $P < 0.05$.

187 To determine if the remaining surface-attached cells were viable, we directly measured the viability of
188 surface-attached cells before and after gentamicin treatment, by LIVE/DEAD staining and quantified
189 the number of cells within 5 independent fields of view. We find that without gentamicin and compared
190 to the WT, the Δ*recA* strain had ~ 2-fold more viable surface-attached cells (Table 1). The gentamicin
191 treated biofilms (Table 1) shows that Δ*recA* cells in a biofilm survive approximately 4-fold better than
192 WT cells upon antibiotic exposure (Table 1). Taken together, the evidence indicates that biofilms made
193 by Δ*recA* protect cells from antibiotic treatment.

194

195 **Increasing RecA diminishes biofilm formation**

196 Together, our data suggest that there is an inverse relationship between RecA and biofilms in *A.*
197 *baumannii.* To further test this relationship, we artificially increased RecA levels in the WT cells and
198 expected that a RecA overproducing strain would form poor biofilms with fewer surface-attached cells
199 than WT or Δ*recA* biofilms. Thus, we introduced the plasmid borne copy of *recA* under its own
200 promoter (pNLAC1-*recA,* Table S1) into the WT strain, which we refer to as $recA^{++}$ (Table S1). We
201 first measured the intracellular RecA concentration of $recA^{++}$ relative to the WT strain. To do this, we
202 purified *A. baumannii* RecA and *Escherichia coli* RecA to test whether an antibody raised against *E.*
203 *coli* RecA recognizes *A. baumannii* RecA equally well. There is no difference between the detection
204 of the *E. coli* RecA or *A. baumannii* RecA for the antibody (Fig. S4A&B). Using semi-quantitative
205 western blot analysis, we found that the relative level of RecA in $recA^{++}$ cells were between 3- to 5-
206 fold higher than WT in both basal and DNA-damage inducing conditions than the parental strain (Fig.
207 S4C). We calculated that after DNA damage, RecA relative levels in the WT strain increased by ~3-
208 fold relative to basal. Thus, $recA^{++}$ at basal conditions has similar levels of RecA as the WT strain
209 treated with 10X MIC of ciprofloxacin (Fig. S4C).

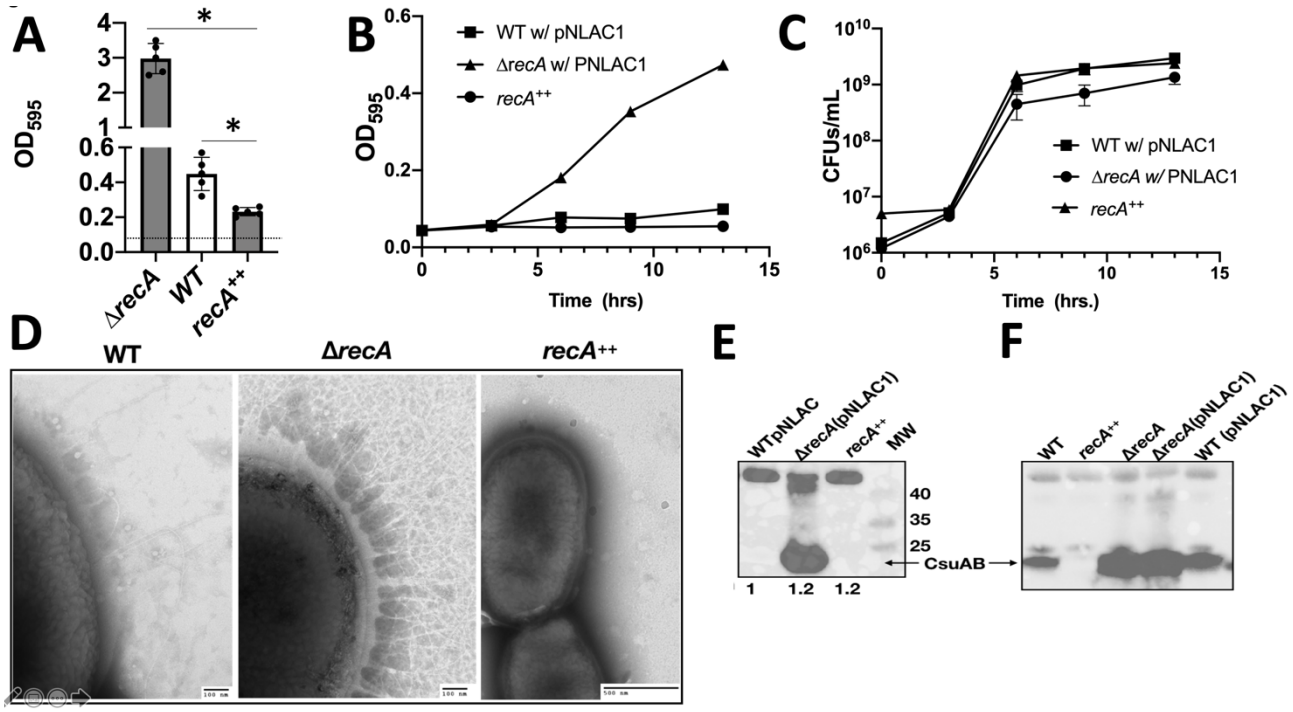

Figure 3. RecA levels modulate *A. baumannii* cell attachment. (**A**) Cells with high levels of RecA form significantly weaker biofilms than Δ*recA* and WT. To change the levels of RecA, we introduced into WT cells a plasmid encoding *recA* driven by its own promoter. We refer to this strain as *recA*$^{++}$. These cells produce RecA at levels similar of fully induced WT cells (Fig. S4). Both WT and Δ*recA* adhere significantly better to surfaces than *recA*$^{++}$. Graph displays absorbance at 595 nm for Crystal Violet staining of polystyrene surface-adhered cells from 48 hr pellicles. The error bars represent the standard deviation of the mean. An unpaired two-tailed T-test was performed for statistical analysis in which Δ*recA* was compared pairwise to each WT and *recA*$^{++}$, and WT was compared to *recA*$^{++}$. * = P < 0.05. **(B)** Δ*recA* cells attach to surfaces faster than either WT or *recA*$^{++}$. Surface attachment of WT (with empty PNLAC1 plasmid), Δ*recA* (with empty PNLAC1 plasmid) and *recA*$^{++}$. Δ*recA* cells attach to polysterene surfaces between 3-6 hours after inoculation. Error bars, for the most part not visible (very small), represent the standard deviation of the mean. (**C**) There is no large difference in growth between strains during the first 13 hrs of biofilm formation. Colony Forming Units (CFUs)/mL of the respective strains at the same time points as in (B). The error bars represent standard deviation of the mean. Experiment was performed in technical triplicate and biological duplicate. (**D**) The Δ*recA* strain has high density of pili. Transmission electron microscopy images of the pili on the surface of the WT, Δ*recA*, and *recA*$^{++}$ strains. The scale bar for the WT and Δ*recA* strains images is 100 nm and 500 nm for *recA*$^{++}$. (**E**) Immunoblot for Csu pili isolated from the indicated strains. The total protein ratio of each cell extract from which the pili were isolated compared to WT is shown at the bottom of the image. The >40kD band is non-specific but clearly shows that same amounts of proteins were loaded per lane. (**F**) Immunoblot for Csu pili from whole cell extracts also show that Δ*recA* cells have more Csu pili. There is no difference in Csu pili between Δ*recA* cells with or without the empty vector (pNLAC1). The cell free extracts were loaded at similar concentrations (20 µg of total protein per lane) as also shown by the >40kD band. An anti-Csu polyclonal primary antibody, and an anti-rabbit secondary antibody were used at the dilutions indicated in Materials and Methods. Lanes are appropriately labelled, and the MW size markers are shown. The CsuAB protein band is highlighted by the arrows.

210 We observed that *recA*$^{++}$ biofilms had significantly less surface-attached cells compared to the WT and

211 Δ*recA* biofilms, but still above the limit of detection (Fig 3A, dashed line shows limit of detection).

212 The *recA*$^{++}$ strain grown in planktonic conditions had a slight growth defect which was like Δ*recA* cells
213 in shaking conditions. These strains doubling time was 0.15X slower than WT based on these growth
214 curves (Fig. S1 C&D).

215

216 **RecA levels influence surface attachment**

217 Since there were minor growth defects in planktonic shaking conditions for Δ*recA* and *recA*$^{++}$ cells
218 (Fig. S1) in the conditions tested, we decided to concurrently measure biofilm attachment and bacterial
219 growth in the first 13 hours of static growth conditions. We inferred that difference in biofilms due to
220 growth would be apparent at the early stages of biofilm formation where there may still be active cell
221 division. To do this, we set up biofilms as indicated in materials and methods and measured surface
222 attachment while also determining colony forming units (CFUs) from 0-13 hrs at regular intervals.
223 Strikingly, at 6 hrs we detected an increase in surface-attached cells for Δ*recA* compared to WT and
224 *recA*$^{++}$, both of which showed little attachment (Fig. 3B). The colony forming unit counts were
225 comparable for all the strains (Fig. 3C). These data show that Δ*recA* cells attach to surfaces earlier than
226 the WT or the *recA*$^{++}$ strains, as our previous assays suggested (Fig. 1B). This also demonstrates that
227 our findings for biofilm formation are directly comparable and not, in part, due to growth differences.
228 In this experiment, as well as in the one shown previously (Fig. 1B), strains contained the empty
229 plasmid (pNLAC1; Table S1) for direct comparison to the complemented strain. We observed that
230 regardless of pNLAC1 (Fig. 3B, C) Δ*recA* forms robust biofilms, while WT and *recA*$^{++}$ do not. Overall
231 our data indicates an inverse relationship between RecA and biofilm development.

232

233 **RecA levels influence density of attachment pili**

234 Since Δ*recA* cells attaches to surfaces faster than WT or *recA*$^{++}$ (Fig. 3A, B), we wanted to investigate
235 whether Δ*recA* had more surface pili to permit attachment. Csu pili are involved in cell adherence in
236 *A. baumannii* biofilms (Gaddy and Actis, 2009; Pakharukova et al., 2018; Rumbo-Feal et al., 2013;
237 Tomaras et al., 2003). To investigate this, we imaged the Δ*recA*, WT and *recA*$^{++}$ strains from saturated
238 cultures using transmission electron microscopy (TEM). Remarkably, Δ*recA* cells displayed a higher
239 density of surface pili than WT or *recA*$^{++}$ cells (Fig. 3D). To determine whether we were observing, in
240 part, Csu pili, we performed a Western blot to detect CsuAB protein from both purified pili (Fig. 3E)
241 and total cell extracts (Fig. 3F). We detected a strong signal for CsuAB pili in Δ*recA* cells.

242

243 We next constructed a plasmid containing the promoter of the *csuAB* operon fused to *gfp* (P_{csuAB}-*gfp*)
244 which was introduced into Δ*recA*, WT, and *recA*$^{++}$ strains. Fluorescence measurements of statically
245 grown cells in YT medium showed a fluorescence signal in Δ*recA* cells at ~6 hours, and the signal
246 further accumulated to orders of magnitude more than WT or *recA*$^{++}$ (Fig. 4A). Indeed, GFP
247 fluorescence of the WT strain with the same *csu* reporter plasmid was detected after 36 hours and
248 gradually increased with time. Expression in the *recA*$^{++}$ strain was even lower, while growth is
249 comparable (Fig. 4A). Single cell imaging of these cells at 20 hrs showed that fluorescence was easily
250 detectable in Δ*recA*, but largely absent in WT or *recA*$^{++}$ (Fig. 4B). Quantification of fluorescence of
251 single cells (Fig. 4C) shows significantly elevated average fluorescence in Δ*recA* cells compared to
252 *recA*$^{++}$ or WT. Notably, *recA*$^{++}$ fluorescence is significantly lower than the WT (Fig. 4C). We next
253 measured expression levels of *csu* pili genes in biofilm pellicle cells using qPCR. *csuAB* expression is
254 ~80-fold higher in *A. baumannii* Δ*recA* and lower in *recA*$^{++}$ compared to WT cells (Fig. 4D). In

255 summary, our data suggested that Δ*recA* cells have deregulated CsuAB pili, which leads to faster

256 surface attachment compared to *recA*$^{++}$ or WT.

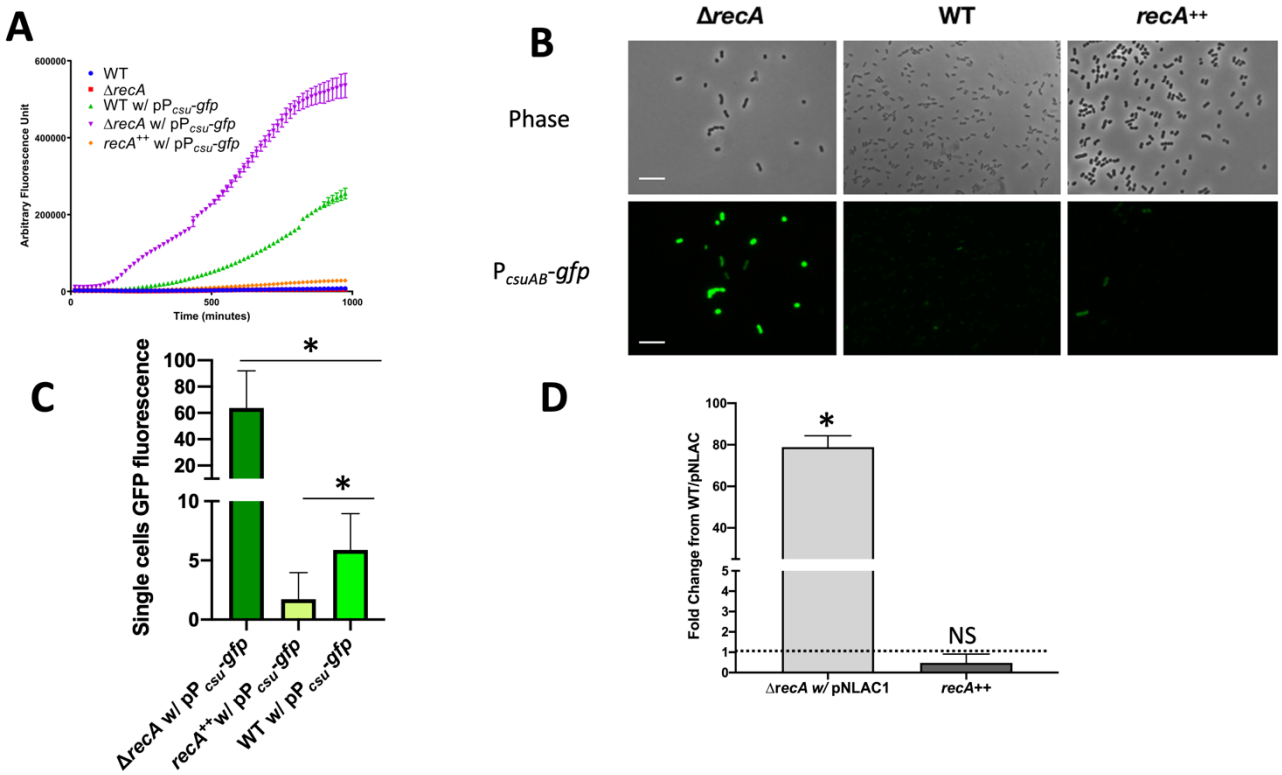

Figure 4. Csu pili expression depends on RecA levels. (A) Δ*recA* cells with a Csu fluorescent reporter show elevated and earlier fluorescence compared to WT or *recA*$^{++}$. Fluorescence, a measure of Csu pili expression, was measured every 15 mins for a 1000 mins at 25ºC in static conditions in a plate reader. (**B**) Single cell detection of the *csu*-gfp reporter shows high *csu* in Δ*recA* cells. Representative fluorescent images of the *A. baumannii* strains with a Csu fluorescent reporter after 24 hrs in shaking conditions. Scale bar represents 10 µm**.** (**C**) Quantification of fluorescence in single cells demonstrate *csu*-gfp fluorescence dependence on RecA levels; high in Δ*recA*, and low in *recA*$^{++}$. At least 300 single cells were counted, and their fluorescence measured with MicrobeJ (Ducret et al., 2016) from microscope images taken with the same settings. Mean single cell fluorescence with standard deviation is plotted. An unpaired two-tailed T-test was performed for statistical analysis; *p<0.05 (**D**) *csu* transcript is higher in Δ*recA* cells compared to WT and *recA*$^{++}$. qPCR was performed in triplicate with three biological repeats to measure *csu* gene expression from the WT, Δ*recA* and *recA*$^{++}$ strains. Expression was standardized to 16S rRNA expression, and the value for the WT strain was set to 1 (dotted line). Error bars represent standard deviation of the mean. An unpaired two-tailed T-Test was used for statistical analysis, compared to gene expression of the WT strain. *= P< 0.05, NS = not significant.

257

258

259 **RecA levels and *csuAB* expression are inversely correlated in DNA-damaged biofilm pellicles**

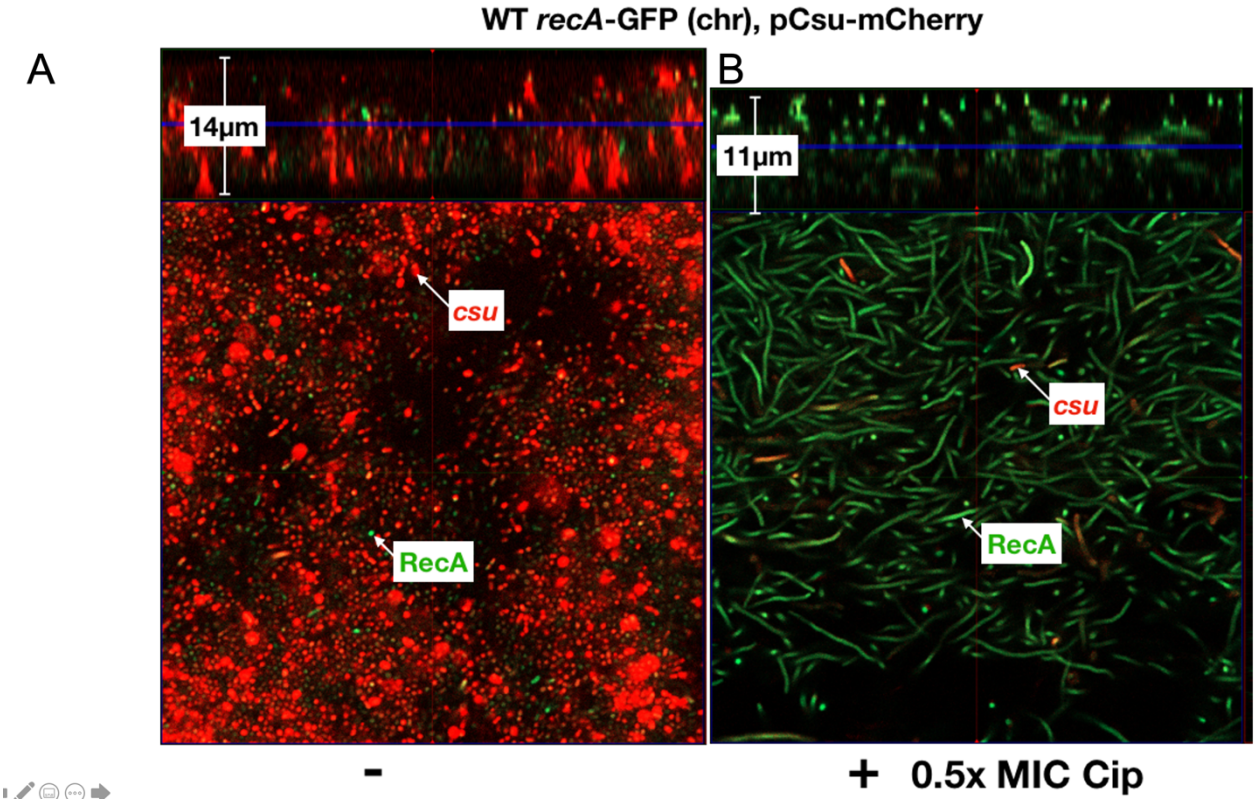

Figure 5. High RecA levels in response to DNA damage lead to thinner biofilms. (**A**) Csu pili are highly expressed in biofilm cells. Confocal microscope imaging of a double label *recA*-GFP (Ching et al., 2018) and *csu* mCherry strain. The thickness of the biofilm in the mid-Z stack is 14µm as shown in the left-hand side of the figure. There are only a few RecA expressing cells. Csu and RecA cells are labeled in the image. (**B**) RecA levels are high in 48 hr treated pellicle biofilms. Treatment with sublethal concentrations of Cip (ciprofloxacin; 0.5X MIC) is enough to induce the DDR (MacGuire et al., 2014), but avoid cell killing. DNA damaged biofilm pellicles images show elongated cells, thinning of the pellicle (mid-Z stack 11µm) and fewer *csu* expressing cells. Representative images were obtained from a Zeiss Axio Observer.Z1/7 with an excitation/emission of 280/618 for the red channel and of 488/509 for the green channel.

260

261 Our findings suggest that increased RecA, which occurs upon DDR induction, will result in decreased

262 biofilms. Due to the absence of a LexA homologue in *A. baumannii*, it is possible that RecA may serve

263 different regulatory roles as has been previously suggested (Hare et al., 2014). Our results suggest that

264 elevated levels of RecA leads to decreased CsuAB pili (Figs. 3-4). Thus, we hypothesized *csuAB*

265 expression would decrease in biofilm cells upon treatment with DNA damage, which leads to an

266 increase in RecA. To test this and monitor both RecA and *csuAB* expression we constructed a plasmid
267 borne transcriptional reporter of Csu genes as the one we used previously (Fig. 4), but used instead

268

269 mCherry, P_{csuAB}-*mCherry* , and we introduced it into the *A. baumannii* strain already containing a
270 chromosomal P_{recA}-*gfp* reporter (Ching et al., 2018). 48 hr pellicle biofilms of the double reporter strain
271 were treated with 0.5X MIC of ciprofloxacin (Cip), which is known to induce the DDR but does not
272 kill cells (MacGuire et al., 2014), for an additional 48 hrs. The biofilm pellicles were examined by
273 confocal microscopy to observe differences in gene expression, and in biofilm thickness.

274 In untreated biofilms (Fig. 5A), most cells had moderate to high expression of the P_{csuAB}-*mCherry* pili
275 reporter with few expressing the P_{recA}-*gfp* (Fig. 5A). In comparison, cells isolated from Cip-treated
276 biofilms showed dramatic changes (Fig. 5B). Most of the DNA damaged biofilm cells were fluorescing
277 GFP, an indication of RecA induction, with few cells expressing mCherry. There appeared to be little
278 to no overlap in gene expression between the two reporters, suggestive of mutually exclusive cell types.
279 Most treated cells were also elongated, as cell division inhibition is a common feature of DDR
280 induction (Kreuzer, 2013). Notably, the untreated pellicles showed high cell density and had a greater
281 thickness (28 µm) than the treated pellicles (22 µm), suggesting that biofilm dispersal occurred in
282 response to DNA damage treatment. It is unlikely that thinning is due to cell death by the Cip treatment
283 since we used sub-MIC levels of Cip. Our data suggest that RecA negatively influences expression of
284 Csu pili genes, necessary for expression of the Csu pili machinery and biofilm formation.

285

286 **RecA levels modulate *bfmR* expression**

287 Csu pili regulation is dependent on BfmR, a key regulator of biofilm formation in *A. baumannii*
288 (Tomaras et al., 2008). Increased Csu pili in Δ*recA* suggests either higher *bfmR* expression or perhaps
289 a more active BfmR. To test whether *bfmR* was differentially expressed we measured expression levels
290 of *bfmR* in biofilm pellicles using qPCR. We found that *bfmR* expression is significantly higher in
291 Δ*recA*, but not in *recA*$^{++}$, compared to WT (~4 folds, Fig. 6A). These results suggest that RecA levels
292 manage *bfmR* expression that in turn controls Csu pili.

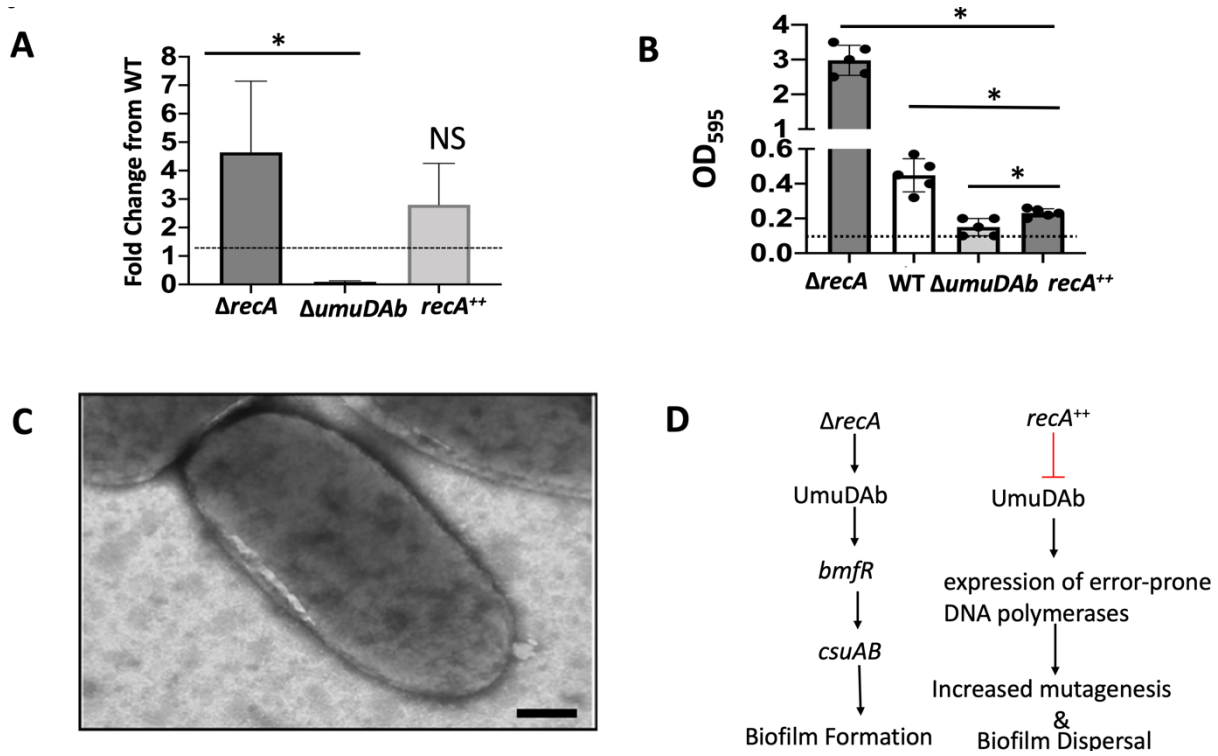

Figure 6. RecA levels modulate biolfilm development through *bfmR* and UmuDAb. (**A**) Δ*recA* have significantly higher *bfmR* expression, the global biofilm regulator. *bfmR* transcript is higher in Δ*recA* compared to WT or *umuDAb*. qPCR was performed twice each with three biological repeats. Dotted line represents WT expression. An unpaired two-tailed T-test was performed for statistical analysis, compared to gene expression of the WT strain; *p<0.05, NS=not significant. (**B**) UmuDAb is the RecA-controlled transcription factor regulating biofilms. A strain lacking *umuDAb* form poor biofilms compared to other strains. The Δ*recA* strain forms biofilm significantly better than any of the other strains tested in pairwise statistical analysis shown by the straight line on top of the columns. The WT strain is significantly different to Δ*umuDAb* and *recA*$^{++}$, while Δ*umuDAb* is significantly different to *recA*$^{++}$. An unpaired two-tailed T-test was performed for statistical analysis; *p<0.05. (**C**) Transmission electron micrograph of the Δ*umuDAb* strain shows no surface pili. Representative image shown. Scale bar is 100nm. (**D**) Model based on the presented data. Arrows represent positive effect while the red blunted line represents a negative effect, which in the UmudAb case we believe is post-translational.

293 **UmuDAb, a RecA-dependent transcription factor, regulates BfmR**

294 While *A. baumannii* lacks LexA, UmuDAb, is a known repressor of some, but not all, DDR genes
295 (Hare et al., 2014). Notably, UmuDAb has a typical helix-turn-helix DNA binding motif at the amino-
296 terminal end that is cleaved by activated RecA nucleoprotein filament, RecA*, in a way believed to be
297 like that of LexA and other proteins within the same family (Draughn et al., 2018; Hare et al., 2013).
298 Cleavage of UmuDAb by RecA* provides a plausible mechanistic explanation for the observations
299 that high RecA levels (i.e. low UmuDAb) lead to biofilm dispersal. Thus, we hypothesized that
300 UmuDAb may serve as a RecA-dependent regulator of biofilms.

301

302 We constructed a Δ*umuDAb* strain as we have previously done (Norton et al., 2013) and tested biofilm
303 formation. We found that the Δ*umuDAb* strain formed significantly weaker biofilms than any of the
304 other strains previously studied in pairwise comparisons (Fig 6B). In fact, Δ*umuDAb* formed
305 significantly worse biofilms than *recA*$^{++}$ (Fig. 6B). Consistent with this observation, TEM showed no
306 visible pili on the surface of Δ*umuDAb* cells (Fig 6C). Furthermore, we detected almost no *bfmR*
307 transcript in Δ*umuDAb* cells compared to WT (Fig 6A). Contrary to the known UmuDAb repressor
308 function (Hare et al., 2014; Witkowski et al., 2016), our findings suggest that UmuDAb has a positive
309 effect on *bfmR* and consequently on *csu*. Taken together, our data suggest that UmuDAb is an inducer
310 of *bfmR*. Our group is currently investigating the mechanism by which UmuDAb performs this
311 function.

312

313 **Discussion**

314 Bacteria largely exist in the environment as biofilms (Costerton et al., 1995). Generally, cells in
315 biofilms have different characteristics and gene expression profiles from their free-living planktonic
316 counterparts. Here, we find that in *A. baumannii* ATCC 17978, RecA levels, a key DDR gene product,

317 influences biofilm development in either the ATCC 17978 (Figs. 1-6) or AB5075 (Fig. S3) strains. Our
318 data also show that cells lacking *recA* produce robust biofilms (Fig. 1). Importantly, Δ*recA* biofilms
319 on an abiotic surface are more resilient (Fig. 2) and are viable after antibiotic treatment (Table 1)
320 providing additional evidence to the concept that biofilms protect cells from antibiotic exposure
321 (Anderl and Franklin, 2000; Singh et al., 2016). Thus, recurring *A. baumannii* infections may be the
322 product of cells remaining adhered to equipment surfaces or implanted devices.

323

324 We found that RecA levels influence biofilm formation through Csu pili density. Δ*recA* cell adherence
325 is dependent on higher *csuAB* and increased Csu pili compared to either the WT or the *recA*$^{++}$ strains
326 (Figs. 3, 4). Our results further suggest that *csuAB* expression is due to induction of *bfmR* (Fig. 6). It
327 has been previously shown that *bfmR* and *csuAB* expression is higher in biofilm cells (Rumbo-Feal et
328 al., 2013) consistent with our findings.

329

330 Aranda *et al.* phenotypically characterized the *ΔrecA* insertional mutant used in this study. Free-living
331 *ΔrecA* cells had decreased survival during heat shock, desiccation, UV, and certain antibiotic treatment
332 (Aranda et al., 2011). Importantly, the *ΔrecA* strain had much lower pathogenicity in a mouse model,
333 indicating its importance in this process (Aranda et al., 2011). These results demonstrate the
334 significance of RecA in survival and virulence in free-living planktonic cells. However, our findings
335 demonstrate the importance of investigating both biofilm and free-living states. For example, it has
336 been shown that strong *A. baumannii* biofilm formers are less frequently antibiotic-resistant, consistent
337 with having lower levels of RecA and subsequently mutagenesis (Wang et al., 2018). Moreover,
338 biofilm cells were more resistant to eradication (Wang et al., 2018), again consistent with the
339 observation that Δ*recA* surface-attached cells are more difficult to eradicate with antibiotics (Fig. 2,

340 and Table 1). For example, certain antibiotics have lowered penetration of biofilms (Anderl and
341 Franklin, 2000; Singh et al., 2016) and there is a nutrient gradient within the biofilm which leads to
342 different metabolic states of biofilm cells (Werner et al., 2004). Additionally, planktonic free-living
343 cells have been shown to more readily gain higher level antibiotic resistances compared to biofilm cells
344 during exposure to ciprofloxacin (Santos-Lopez et al., 2019).
345

346 Our findings have significant implications on understanding *A. baumannii* survival to antibiotic
347 treatment and possibly antibiotic resistance. We show that upon DNA damage, the DNA damage
348 response is induced, leading to induction of *recA* with simultaneous shutoff of biofilm genes, leading
349 to thinner biofilms (Fig. 5). We have observed that this occurs through lowered *bfmR* and *csuAB*
350 expression upon elevated RecA levels. Quantification of RecA upon DNA damage, and in $recA^{++}$ cells,
351 demonstrates how sensitive biofilm gene expression is to a change in RecA levels (Figs. S4, 1-3). This
352 may be due to the UmuDAb sensitivity to cleavage by RecA* (Hare et al., 2013).

353

354 Our evidence suggests that UmuDAb is an inducer of *bfmR* and of biofilm formation (Fig. 6). A
355 summary and model of genes is shown in Fig. 6D. Based on previous findings, we have observed
356 bimodality of *recA* expression in planktonic cells (Ching et al., 2017; MacGuire et al., 2014), and there
357 may also be heterogeneity in RecA levels between cells in biofilms. Thus, within the biofilm there may
358 be two cell types: $RecA^{Low}$ cells maintain biofilms and low mutagenic potential while $RecA^{High}$ cells
359 with high mutagenic potential (Norton et al., 2013) can disperse and search for new niches. This
360 observed inverse relationship can allow the population to combine physical (biofilm) and genetic
361 (elevated mutagenesis) protection to environmental challenges, including antibiotic exposure in a host.

362

363 Overall, we have identified an inverse relationship between the DDR and biofilm development in *A.*
364 *baumannii.* These results demonstrate the complexity of treating pathogens with a DDR that does not
365 follow the paradigm, such as *A. baumannii* (Ching et al., 2017; MacGuire et al., 2014). Recent work
366 has highlighted the potential for clinical RecA inhibitors to potentiate the effect of antibiotics while
367 hindering antibiotic resistance acquisition by reducing mutagenic capacity in bacteria (Alam et al.,
368 2016). This indeed may be promising in the treatment of certain bacteria, as demonstrated in *E. coli*
369 (Alam et al., 2016). However, our results show that for *A. baumannii*, inhibiting RecA may lead to
370 robust biofilm formation. It is thus important to understand the relationships between survival strategies
371 in bacteria, and that different bacteria may have different responses to treatment, based on their
372 fundamental biology. Overall, our results show the complex ways that *A. baumannii* robustly survives
373 stress by balancing alternative survival strategies.

374

375 **Methods**

376 **Strains and Growth Conditions**

377 Strains and plasmids used are listed in Table S1. *A. baumannii* strains harboring the PNLAC1-*recA*
378 plasmid were constructed as before (Ching et al., 2017). The Δ*umuDAb* strain was constructed using
379 SOE PCR to insert a kanamycin gene cassette in the *umuDAb* gene as before (Norton et al., 2013). The
380 oligonucleotides used are in Table S1. All bacterial cultures were routinely grown in LB medium,
381 unless otherwise noted, and incubated at 37°C with shaking at 225 rpm for liquid cultures. YT medium
382 used is composed of 2.5g NaCl, 10g Tryptone and 1g Yeast extract per liter. Solid medium contains
383 1.5% agar (Fisher Bio-Reagents). Antibiotics were used at the following concentrations: Kanamycin
384 (Kan; 35 µg/mL), Gentamicin (Gm; 10 µg/mL), Tetracycline (Tet; 12 µg/mL) and Carbenicillin (Carb;
385 100 µg/mL).

386 **Growth curve measurements**

387 Strains were diluted in the growth medium as indicated in the respective figure legends and grown in
388 YT medium in 96-well dishes. All strains were grown at least in triplicate. They were incubated in a
389 plate reader (Biotek Synergy H1) at 37ºC with shaking for 24 hrs. with measurements of OD_{600} every
390 15 mins.

391 **Pellicle & Colony Biofilm Formation**

392 To form pellicle biofilms, cells from a saturated culture were inoculated at a 1:1000 dilution into YT
393 liquid medium in either 6, 12 or 24-well non-tissue culture treated (lacking coating which change
394 surface properties) polystyrene plates. The same number of cells, adjusted based on optical density,
395 were added to each well. Plates were then incubated statically at 25°C. A standard Crystal violet
396 staining procedure was used to quantify adherence to the polystyrene surface (Chen et al., 2015). Early
397 biofilms are formed after 24 hrs of static growth and between 48-72 hrs. the biofilm has matured. After
398 72 hrs. the biofilms start to deteriorate. In the time course experiment, to correlate viable cells and
399 biofilm formation, samples were taken for CFU counting from 3 wells per experiment. The well content
400 was thoroughly mixed before taking the samples, diluted with PBS, and plated on LB agar. After CFU
401 sampling, the well content was aspirated, washed 3 times with PBS, and stained with Crystal Violet as
402 before (Ching et al., 2018). For colony biofilms, 3 µL of a saturated bacterial culture were spotted on
403 to YT agar plates containing 200µg/mL Congo red and 100µg/mL Coomassie brilliant blue (Congo
404 red plates) (Ching et al., 2018) and incubated for 48 hrs., early colony biofilms, to 96 hrs. at 25°C.
405 Images of biofilms were taken with a Leica MSV269 dissecting scope and a Leica DMC2900 camera,
406 using the same settings. The radius of the biofilm colonies was measured in triplicate from the
407 dissecting microscope images at the same magnification.

408

409 **Scanning Electron (SEM) and Transmission Electron (TEM) microscopy**

410 Biofilms for SEM were prepared by collecting pellicle biofilms on a glass coverslip treated with a
411 solution of 0.1 mg/mL of polylysine (Fisher Scientific). The coverslips with the biofilms were
412 deposited for at least 24 hrs at 4ºC in wells with fixative 1 composed of 25% Glutaraldehyde, 0.1 M
413 Na-Cacodylate buffer (pH 7.2), 0.15% Alcian Blue and 0.15% Safranin. Additional treatment of the
414 coverslips and observation of the biofilms was performed at the Northeastern University Electron
415 Microscopy Core Facility.

416 For TEM, cultures were grown to saturation in YT liquid medium and streaked for single colonies on
417 YT plates incubated at 37°C. A colony was picked and gently resuspended in 100 µL of phosphate
418 buffered saline (PBS). 10 µL of the resuspended colony was pipetted onto a copper grid, excess liquid
419 wicked away with filter paper, and the grid was dried at room temperature. To negatively stain the
420 samples and observe pili, 10 µL of a solution of 1.5% phosphotungstic acid (PTA) was pipetted onto
421 the cell-containing grids. Liquid excess was wicked away with filter paper, and grids were left to air
422 dry at room temperature. Microscopy was performed with a JEOL JEM-1010 (JEOL USA, Peabody,
423 MA) microscope equipped with a 2k x 2k AMT CCD camera (Advanced Microscopy Techniques,
424 Woburn, MA) at the Northeastern University Electron Microscopy Core Facility.

425

426 **Quantitative measurement of gene expression**

427 To measure *bfmR* and *csu* transcripts in WT, Δ*recA*, and *recA*$^{++}$, we took 500µL of 48 h statically
428 grown pellicle cells. These were harvested by centrifugation and resuspended in 1 mL of RNA Protect
429 Bacteria Reagent (Qiagen) with 30µL of 20 mg/mL lysozyme, incubated at room temperature for 15
430 min, spun down at 15,000g for 5 min, and cell pellets were stored at -20 ºC. Total RNA extraction was

431 carried out by using the Zymo Direct-zol RNA Kit (Zymo) according to manufacturer's instructions.
432 A NanoDrop One (ThermoFisher) was used to measure RNA concentration and purity. RNA was
433 converted to cDNA using a high capacity cDNA reverse transcription kit according to the
434 manufacturer's protocol (Applied Biosystems). Expression of *bfmR* and *csuAB* pili gene expression by
435 RT-qPCR was performed with cDNA using the qPCR primer pairs listed in Table S1 and following
436 the protocol for Fast SYBR Green Master Mix (Applied Biosystems) using a StepOnePlus real-time
437 PCR instrument (Applied Biosystems). Relative gene expression was standardized using endogenous
438 16S ribosomal RNA expression and the comparative threshold cycle (ΔΔCT) was calculated for each
439 sample and compared relative to WT expression. Experiments were repeated twice, and each sample
440 was run in biological triplicate. An unpaired two tail T test was used for statistical analysis relative to
441 the parental strain (*=$P < 0.05$).

442

443 **Pilus purification.**

444 Pilus shear preparations were performed as previously published (Moon et al., 2017). Briefly, similar
445 number of cells grown on a YT agar plate (OD_{600}~20) were collected in 1.5 mL of 1X PBS, placed on
446 ice for 10 min, and vortexed for 1 min. After centrifugation at 13,000 x g at 4ºC, cells supernatants
447 (containing the pili) and the respective pellets (containing pili-less cells) were collected. The pili within
448 supernatants were precipitated for 20 hrs with trichloroacetic acid (TCA) (final concentration, 25%),
449 at -20°C. The precipitated pili were collected by centrifugation at 16,000 x g for 10 min at 4°C and
450 resuspended in 50 µL 1X PBS. Total protein was extracted from pili-free cell pellets and whole cell
451 lysates using Bugbuster reagent (Novagen) following the manufacturer's instructions and quantified
452 using a Bradford assay.

453 **Purification of His-tagged *A. baumannii* RecA and Immunoblots**

454 The *recA* gene from *A. baumannii* was amplified using primers RecALICF and RecALICR (Table S1)
455 and cloned into the pET-His6-TEV-LIC vector (plasmid 29653; Addgene, Cambridge, MA, USA)
456 using Ligation Independent Cloning Protocol (Gradia et al., 2017) and introduced by transformation
457 into DH5α *Escherichia coli* cells for plasmid maintenance. The induction of expression and
458 purification methods are as previously described for RecA purification from *Escherichia coli* (Tashjian
459 et al., 2017). RecA purification was confirmed by SDS-PAGE.

460

461 For the semi-quantitative western blots, saturated cultures were diluted 1:100 and grown to exponential
462 phase. Cells were then treated with ciprofloxacin (Cip) at 10X the MIC for 3 hrs (Ching et al., 2017).
463 A parallel culture for each strain was left untreated. Cells were collected by centrifugation and whole-
464 protein lysate was extracted using Bugbuster reagent (Novagen) and Pierce Universal Nuclease
465 according to manufacturer's instructions. Cell free lysates were quantified with a Bradford assay
466 following manufacturer's instructions (BioRad). Lysate was diluted to 1X with Laemmli buffer and
467 heated for 10 minutes at 95ºC. The samples were separated on a 12% Bis-Tris gel (Invitrogen) in MOPS
468 buffer and transferred to a nitrocellulose membrane (Cafarelli et al., 2013). The blot was developed as
469 before (Cafarelli et al., 2013) using a primary anti-RecA antibody (Abcam) at a 1:10,000 dilution
470 (Norton et al., 2013) and an HRP-labelled secondary goat anti-rabbit antibody (Abcam) diluted at
471 1:40,000. The density of the RecA bands was quantified by ImageJ (Norton et al., 2013). The RecA
472 signal from all samples were compared to a standard of purified RecA protein from *A. baumannii*.
473 Similar loading of lanes was measured by Commassie Blue staining of a parallel gel. The procedure
474 was done in 4 biological replicates. RecA determinations were similar every time.

475

476 To measure the relative amount of Csu pili in the different strains, we performed immunoblots with an
477 anti-Csu antibody (gracious gift from Luis Actis). The pili content of each strain was standardized to
478 the total protein measured in the cell-free extracts from which the pili were isolated. To detect Csu pili
479 from whole cell lysates, similar number of cells were lysed with Bugbuster and Pierce Universal
480 Nuclease as indicated above. The samples were separated in a 12% polyacrylamide gel in MES buffer
481 at 150V for 1 hour. Immunoblot procedures were followed as above using a 1:1000 dilution of the anti-
482 Csu primary antiserum and a 1:40,000 dilution of the HRP labeled secondary anti-rabbit antibody
483 (Abcam). A ChemiDoc MP imaging system (BioRad) was used for chemiluminescence signal
484 detection from RecA and Csu blots.

485

486 **Construction of the P_{csu}-*gfp* and P_{csu}-*mCherry* expression reporter plasmids and expression**
487 **assays**

488 *A. baumannii* ATCC 17978 containing a *csu* operon (P_{csu}-*gfp*) transcriptional reporter on the
489 Carbenicillin (Carb) resistant plasmid pTU1-A-AB (Moore et al., 2016) was used to assess the
490 expression of Csu in the WT, *recA*$^{++}$ and Δ*recA* strains. The P_{csu}-*gfp* reporter plasmid was made
491 utilizing a modified version of the EcoFlex Kit (Moore et al., 2016). The EcoFlex kit was a gift from
492 Paul Freemont (Addgene kit #1000000080). All level 1-3 plasmids (Addgene accession numbers
493 72935-72946) were digested with PstI and dephosphorylated using Quick CIP (both New England
494 Biolabs, Ipswich, MA.). PstI restriction sites were attached to the *A. calcoaceticus'* native pWH1266
495 backbone by PCR amplification with primers ori_ab_pstI_r and ori_ab_pstI_f (Table S1). The
496 amplicon was further digested with PstI and ligated using T4 DNA ligase (Thermo Fisher Scientific)
497 into the linearized level 1-3 plasmids. 5 μL of the ligation mix was introduced by transformation into
498 chemically competent *E. coli* DH5α. Positive clones were confirmed by a digest with PstI and BsaI

499 (New England Biolabs, Ipswich, MA.). Afterwards, the promoter region of the *csu* operon was
500 amplified using primers csu_f and csu_r. The pBP_lacZ (Table S1; Addgene accession number 72948)
501 and the purified PCR fragment were digested using SphI and NdeI and the pBP-lacZ plasmid
502 dephosphorylated. The ligation was carried out with T4 DNA ligase (Thermo Fisher Scientific).
503 Colonies were screened using blue-white color in plates with X-Gal and verified by colony PCR and
504 sequencing using Primers pBP_pTU_f and pBP_r.

505

506 Plasmids with the expected inserts were then used in a combined cloning and ligation reaction, by using
507 20 fmol of each entry vector (pBP_csu, pBP_B0012, pBP_e*gfp*, pBP_pET-RBS and pTU1-A-RFP-
508 AB) combined with 2 µL of Cutsmart, 0.5 µL of BsaI-HFv2, 0.5 µL of T4 DNA Ligase and 1 µL of
509 10 mM ATP (all reagents from New England Biolabs, Ipswich, MA., except T4 DNA Ligase from
510 Thermo Fisher Scientific). The reaction was cycled 50 times in a thermocycler with a 37 °C digestion
511 step for 2 minutes and a 16 °C ligation step for 5 minutes. Any plasmid with no insert is eliminated
512 from the mix by digestion with BsaI at 37 °C for 1 h. The enzymes were heat-inactivated at 80°C for
513 10 min. 5 µL of the ligation mix was introduced by transformation into chemically competent *E. coli*
514 DH5α. Colonies with the expected fragment were screened by red-white color in which white colonies
515 contain the desired insert due to the exchange of the mCherry gene originally in the pTU1-A-AB
516 cloning site and confirmed by colony PCR and sequencing the insert using pBP_pTU_f and pTU_r.
517 Plasmids with the desired constructs were introduced by transformation into *A. baumannii* utilizing
518 standard electroporation protocols(MacGuire et al., 2014). To construct the mCherry *csuAB* reporter,
519 (P_{csu}-*mCherry*) same primers and approach were used except that the plasmid pBP_ORF-mCherry was
520 used instead.

521

522 **Microscopy and GFP reporter measurements**

523 To perform confocal microscopy experiments we used a Zeiss Axio Observer.Z1/7. The
524 excitation/emission used were 280/618 nm for the red channel, and 488/509 nm for the green channel.
525 We formed biofilms in wells, and after 48 hrs, 0.5xMIC Cip was added underneath pellicles and dishes
526 were incubated statically for an additional 48 hrs. Pellicles were collected from mock treated and Cip-
527 treated wells on a glass coverslip treated with 0.1 mg/mL of polylysine to facilitate attachment. The
528 side of the pellicle in direct contact with the liquid medium was in contact with the glass, and the side
529 of the biofilm in contact with air remained as such. Z-stacks were of 1µm.

530

531 For the GFP reporter measurements, GFP fluorescence was measured in a plate reader (Biotek synergy
532 H1) for at least 24 hrs. at 25ºC without shaking. To start the experiment, cultures were diluted 1:100
533 in YT medium in a 96 multi-well dish. Green fluorescence (Excitation 479 nm and emission 520 nm)
534 and OD_{600} were measured every 15 mins. Growth and fluorescence data were gathered at least in
535 triplicate for each strain.

536

537 **MIC and Biofilm Eradication Assays, and Live/Dead determination.**

538 Standard assays were used to test for MIC (Andrews, 2001) in planktonic shaking cultures. Pellicles
539 were set up as described above and incubated statically at 25°C for the number of hours indicated in
540 the respective figure legends, at which time cells that were not stuck to the wells ʼsurface were
541 removed, and wells washed three times with 1X PBS. YT medium containing Gm, at a range of
542 concentrations shown in the respective figures was added to each washed well. The plate was then
543 incubated statically for 24 hrs. at 25°C, after which the spent medium was removed, and wells were
544 washed three times with PBS. Crystal Violet staining was then carried out as before (Chen et al., 2015).

545 LIVE/DEAD staining was performed on resuspended surface-attached cells, and microscopy
546 performed as before (Ching et al., 2018). The LIVE/DEAD stained surface attached cells of the WT,
547 Δ*recA*, and *recA*$^{++}$ after Gm treatment (10X MIC) were mechanically dislodged. This methodology did
548 not affect cells' integrity. The number of total cells obtained from the surface-attached fraction varied
549 from strain to strain due to their difference in ability to attach to surfaces. The total number of cells and
550 their viability was determined by counting 5 independent microscope fields from each of the strains.

551

552 **Competing Interests**

553 The authors declare no competing interests.

554

555 **Author Contributions**

556 V.G.G., and C.C. initiated research in discussions with YC. B. I. performed preliminary experiments.
557 C.C., P.M., A.R., M. B., B. N., S. R., M.D., W. F., and V.G.G. performed experiments and analyzed
558 data. C.C. and V.G.G. wrote the manuscript.

559

560 **Funding**

561 M.D. and S.R. were funded by the Undergraduate Research and Fellowships office at Northeastern
562 University. V.G.G. is funded by a stipend from NUSci, an Inclusive Excellence award form HHMI and
563 the NSF REU site award #1757443, Y.C. is funded by an NSF grant (MCB1651732), and A.R. by
564 Northeastern University Provost Dissertation Completion Fellowship.

565 **Acknowledgments**

566 We would like to acknowledge members of the Godoy, Chai, and Geisinger labs at Northeastern
567 University for helpful comments and discussion. We would like to thank G. Bou from Servicio de
568 Microbiologia, Complejo Hospitalario Universitario, La Coruña, Spain for the Δ*recA* strain, Luis Actis
569 from the Department of Microbiology, Miami University, for the anti-Csu antibody, and Stephen Lory
570 from Harvard Medical School for access to the AB7505 transposon collection.

571 **Table 1. Viability of surface attached cells**

Strain/Treatment	Total number attached live cells*	Ratio to WT
WT/No Gm	1046	**1**
Δ*recA*/No Gm	2366	**2.3**
recA^{++}/No Gm	627	**0.6**
WT/Gm[a]	293	**1**
Δ*recA*/Gm[a]	1046	**3.6**
recA^{++}/Gm[a]	NF	_

572

573 * in 5 fields; [a]15µg/mL; NF, None found

574 **References:**

575 Alam K, Alhhazmi A, Decoteau JF, Luo Y, Geyer CR, Alam K, Alhhazmi A, Decoteau JF, Luo Y,
576 Geyer CR. 2016. RecA Inhibitors Potentiate Antibiotic Activity and Block Evolution of
577 Antibiotic Resistance Article RecA Inhibitors Potentiate Antibiotic Activity and Block
578 Evolution of Antibiotic Resistance. *Cell Chem Biol* **23**:381–391.
579 doi:10.1016/j.chembiol.2016.02.010

580 Anderl JN, Franklin MJ. 2000. Role of Antibiotic Penetration Limitation in Klebsiella pneumoniae
581 Biofilm Resistance to Ampicillin and Ciprofloxacin. *Antimicrob Agents Chemother* **44**:1818–
582 1824.

583 Andrews JM. 2001. Determination of minimum inhibitory concentrations. *J Antimicrob Chemother*
584 5–16.

585 Aranda J, Bardina C, Beceiro A, Rumbo S, Cabral MP, Barbé J, Bou G. 2011. Acinetobacter
586 baumannii RecA protein in repair of DNA damage, antimicrobial resistance, general stress
587 response, and virulence. *J Bacteriol* **193**:3740–7. doi:10.1128/JB.00389-11

588 Asally M, Kittisopikul M, Rue P, Du Y, Hu Z, Cagatay T, Robinson AB, Lu H, Garcia-Ojalvo J, Suel
589 GM. 2012. Localized cell death focuses mechanical forces during 3D patterning in a biofilm.
590 *Proc Natl Acad Sci* **109**:18891–18896. doi:10.1073/pnas.1212429109

591 Bales PM, Renke EM, May SL, Shen Y, Nelson DC. 2013. Purification and Characterization of
592 Biofilm-Associated EPS Exopolysaccharides from ESKAPE Organisms and Other Pathogens.
593 *PLoS One* **8**. doi:10.1371/journal.pone.0067950

594 Blair JMA, Webber MA, Baylay AJ, Ogbolu DO, Piddock LJ V. 2014. Molecular mechanisms of
595 antibiotic resistance. *Nat Rev Microbiol* **13**:42–51. doi:10.1038/nrmicro3380

596 Brossard KA, Campagnari AA. 2012. The Acinetobacter baumannii Biofilm-Associated Protein
597 Plays a Role in Adherence to Human Epithelial Cells. *Infect Immun* 228–233.
598 doi:10.1128/IAI.05913-11

599 Cafarelli TM, Rands TJ, Benson RW, Rudnicki PA, Lin I, Godoy VG. 2013. A single residue unique
600 to dinb-like proteins limits formation of the polymerase IV multiprotein complex in Escherichia
601 coli. *J Bacteriol* **195**:1179–1193. doi:10.1128/JB.01349-12

602 Chen Y, Gozzi K, Yan F, Chai Y. 2015. Acetic acid acts as a volatile signal to stimulate bacterial
603 biofilm formation. *MBio* **6**:1–13. doi:10.1128/mBio.00392-15

604 Ching C, Gozzi K, Heinemann B, Chai Y, Godoy VG. 2017. RNA-Mediated cis Regulation in
605 Acinetobacter baumannii Modulates Stress-Induced Phenotypic Variation. *J Bacteriol* **199**:1–15.

606 Ching C, Yang B, Onwubueke C, Lazinski D, Camilli A, Godoy VG. 2018. Lon protease has
607 multifaceted biological functions in *Acinetobacter baumannii*. *J Bacteriol* **201**:1–12.
608 doi:10.1128/JB.00536-18

609 Choi AH, Slamti L, Avci FY, Pier GB. 2009. The pgaABCD Locus of Acinetobacter baumannii
610 Encodes the Production of Poly- ᴺᴸ -1-6- N -Acetylglucosamine , Which Is Critical for Biofilm
611 Formation . *J Bacteriol* **191**:5953–5963. doi:10.1128/JB.00647-09

612 Cirz RT, Jones MB, Gingles NA, Minogue TD, Jarrahi B, Peterson SN, Romesberg FE. 2007.
613 Complete and SOS-mediated response of Staphylococcus aureus to the Antibiotic
614 Ciprofloxacin. *J Bacteriol* **189**:531–539. doi:10.1128/JB.01464-06

615 Costa SB, Campos ACC, Pereira ACM, Mattos-guaraldi AL De, Ju RH, Rosa P, Asad MBO. 2014.
616 Adherence to abiotic surface induces SOS response in Escherichia coli K-12 strains under

617 aerobic and anaerobic conditions. *Microbiology* 1964–1973. doi:10.1099/mic.0.075317-0

618 Costerton JW, Lewandowski Z, Caldwell DE, Korber DR, Sn S, Lappin-scott HM. 1995. Microbial
619 biofilms. *Annu Rev Microbiol* 711–745.

620 Cox JM, Li H, Wood EA, Chitteni-Pattu S, Inman RB, Cox MM. 2008. Defective dissociation of a
621 "slow" RecA mutant protein imparts an Escherichia coli growth defect. *J Biol Chem* **283**:24909–
622 24921. doi:10.1074/jbc.M803934200

623 Draughn GL, Milton ME, Feldmann EA, Bobay BG, Roth BM, Olson AL, Thompson RJ, Actis LA,
624 Davies C, Cavanagh J. 2018. The Structure of the Biofilm-controlling Response Regulator
625 BfmR from Acinetobacter baumannii Reveals Details of Its DNA-binding Mechanism. *J Mol*
626 *Biol* **430**:806–821. doi:10.1016/j.jmb.2018.02.002

627 Ducret A, Quardokus E, Brun Y. 2016. MicrobeJ, a high throughput tool for quantitative bacterial
628 cell detection and analysis. *Nat Microbiol* **1**:1–7. doi:10.1038/nmicrobiol.2016.77

629 Erlandsen SL, Kristich CJ, Dunny GM, Wells CL. 2004. High-resolution Visualization of the
630 Microbial Glycocalyx with Low-voltage Scanning Electron Microscopy : Dependence on
631 Cationic Dyes The Journal of Histochemistry & Cytochemistry. *J Histochem Cytochem*
632 **52**:1427–1435. doi:10.1369/jhc.4A6428.2004

633 Eze EC, Chenia HY, El Zowalaty ME. 2018. Acinetobacter baumannii biofilms : effects of
634 physicochemical factors , virulence , antibiotic resistance determinants , gene regulation , and
635 future antimicrobial treatments. *Infect Drug Resist* **11**:2277–2299.

636 Farrow JM, Wells G, Pesci EC. 2018. Desiccation tolerance in Acinetobacter baumannii is mediated
637 by the two-component response regulator BfmR. *PLoS One* **13**:1–25.

638 doi:10.1371/journal.pone.0205638

639 Fuchs RP, Fujii S. 2013. Translesion DNA Synthesis and Mutagenesis in Prokaryotes. *Cold Spring*
640 *Harb Perspect Biol* 1–22.

641 Gaddy JA, Actis LA. 2009. Regulation of Acinetobacter baumannii biofilm formation. *Futur*
642 *Microbiol* **4**:273–278. doi:10.2217/fmb.09.5.Regulation

643 Gallagher LA, Ramage E, Weiss EJ, Radey M, Hayden HS, Held KG, Huse HK, Zurawski D V.,
644 Brittnacher MJ, Manoil C. 2015. Resources for Genetic and Genomic Analysis of Emerging
645 Pathogen Acinetobacter baumannii. *J Bacteriol* **197**:2027–2035. doi:10.1128/jb.00131-15

646 Geisinger E, Isberg RR. 2015. Antibiotic Modulation of Capsular Exopolysaccharide and Virulence
647 in Acinetobacter baumannii. *PLoS Pathog* **11**:1–27. doi:10.1371/journal.ppat.1004691

648 Ghodke H, Paudel BP, Lewis JS, Jergic S, Gopal K, Romero ZJ, Wood EA, Woodgate R, Cox MM,
649 Oijen AMV. 2019. Spatial and temporal organization of reca in the escherichia coli dna-damage
650 response. *Elife* **8**:1–37. doi:10.7554/eLife.42761

651 Gozzi K, Ching C, Paruthiyil S, Zhao Y, Godoy VG, Chai Y. 2017. Bacillus subtilis utilizes the DNA
652 damage response to manage multicellular development. *npj Biofilms Microbiomes* **3**:8.
653 doi:10.1038/s41522-017-0016-3

654 Gradia S, Ishida JP, Tsai M, Jeans C, Tainer JA, States U, Bioimaging I, Berkeley L, States U,
655 Berkeley L, States U, States U, States U. 2017. MacroBac: New technologies for robust and
656 efficient large-scale production of recombinant multi-protein complexes. *Methods Enzym*.
657 doi:10.1016/bs.mie.2017.03.008.MacroBac

658 Hardouin J, Chabane YN, Marti S, Rihouey C. 2014. Characterisation of Pellicles Formed by

659 Acinetobacter baumannii at the Air-Liquid Interface. *PLoS One* **9**.
660 doi:10.1371/journal.pone.0111660

661 Hare JM, Adhikari S, Lambert K V, Hare AE, Alison N. 2013. The Acinetobacter regulatory
662 UmuDAb protein cleaves in response to DNA damage with chimeric LexA/UmuD
663 characteristics. *FEMS Microbiol Lett* **334**:57–65. doi:10.1111/j.1574-6968.2012.02618.x.The

664 Hare JM, Ferrell JC, Witkowski T a, Grice AN. 2014. Prophage induction and differential RecA and
665 UmuDAb transcriptome regulation in the DNA damage responses of Acinetobacter baumannii
666 and Acinetobacter baylyi. *PLoS One* **9**:e93861. doi:10.1371/journal.pone.0093861

667 He X, Lu F, Yuan F, Jiang D, Zhao P, Zhu J, Cheng H, Cao J, Lu G. 2015. Biofilm formation caused
668 by clinical acinetobacter baumannii isolates is associated with overexpression of the AdeFGH
669 efflux pump. *Antimicrob Agents Chemother* **59**:4817–4825. doi:10.1128/AAC.00877-15

670 Inagaki S, Fujita K, Nagayama K, Funao J, Effects OT. 2009. Effects of recombinase A deficiency
671 on biofilm formation by Streptococcus mutans. *Oral Microbiol Immunol* 104–108.

672 Jacobs AC, Thompson MG, Black CC. 2014. AB5075 , a Highly Virulent Isolate of Acinetobacter
673 baumannii , as a. *MBio* **5**:1–10. doi:10.1128/mBio.01076-14.Editor

674 Korch SB, Hill TM. 2006. Ectopic overexpression of wild-type and mutant hipA genes in
675 Escherichia coli: Effects on macromolecular synthesis and persister formation. *J Bacteriol*
676 **188**:3826–3836. doi:10.1128/JB.01740-05

677 Kreuzer KN. 2013. DNA Damage Responses in Prokaryotes: Regulating Gene Expression,
678 Modulating Growth Patterns, and Manipulating Replication Forks. *Cold Spring Harb Perspect*
679 *Biol* 1–23.

680 Kuhl SA, Zimmer JA, Rohatgi P. 2003. Complementation of bacteriophage induction and
681 recombination defects in Escherichia coli RecA- mutants by expression of the cloned T4
682 bacteriophage uvsX gene. *Curr Microbiol* **46**:88–93. doi:10.1007/s00284-002-3793-7

683 Linares JF, Gustafsson I, Baquero F, Martinez JL. 2006. Antibiotics as intermicrobial signaling
684 agents. *Proc Natl Acad Sci* **103**.

685 Little JW, Mount DW. 1982. The SOS Regulatory Escherichia coli System of Review **29**:1982.

686 Loehfelm TW, Luke NR, Campagnari AA. 2008. Identification and characterization of an
687 Acinetobacter baumannii biofilm-associated protein. *J Bacteriol* **190**:1036–1044.
688 doi:10.1128/JB.01416-07

689 Luke NR, Sauberan SL, Russo TA, Beanan JM, Olson R, Loehfelm TW, Cox AD, Michael FS,
690 Vinogradov E V, Campagnari AA. 2010. Identification and Characterization of a
691 Glycosyltransferase Involved in Acinetobacter baumannii Lipopolysaccharide Core
692 Biosynthesis . *Infect Immun* **78**:2017–2023. doi:10.1128/IAI.00016-10

693 MacGuire AE, Ching MC, Diamond BH, Kazakov A, Novichkov P, Godoy VG. 2014. Activation of
694 phenotypic subpopulations in response to ciprofloxacin treatment in Acinetobacter baumannii.
695 *Mol Microbiol* **92**:138–52. doi:10.1111/mmi.12541

696 Moon KH, Weber BS, Feldman F. 2017. Subinhibitory Concentrations of Trimethoprim and
697 Sulfamethoxazole Acinetobacter baumannii through Inhibition of Csu Pilus Expression.
698 *Antimicrob Agents Chemother* **61**:1–18.

699 Moore SJ, Lai HE, Kelwick RJR, Chee SM, Bell DJ, Polizzi KM, Freemont PS. 2016. EcoFlex: A
700 Multifunctional MoClo Kit for E. coli Synthetic Biology. *ACS Synth Biol* **5**:1059–1069.

701 doi:10.1021/acssynbio.6b00031

702 Norton MD, Spilkia AJ, Godoy VG. 2013. Antibiotic Resistance Acquired through a DNA Damage-
703 Inducible Response in Acinetobacter baumannii. *J Bacteriol* **195**:1335–45.
704 doi:10.1128/JB.02176-12

705 Pakharukova N, Tuittila M, Paavilainen S, Malmi H, Parilova O, Teneberg S, Knight SD, Zavialov A
706 V. 2018. Structural basis for Acinetobacter baumannii biofilm formation. *Proc Natl Acad Sci U*
707 *S A* **115**:5558–5563. doi:10.1073/pnas.1800961115

708 Peleg AY, Seifert H, Paterson DL. 2008. Acinetobacter baumannii: Emergence of a successful
709 pathogen. *Clin Microbiol Rev* **21**:538–582. doi:10.1128/CMR.00058-07

710 Rice LB. 2008. Federal funding for the study of antimicrobial resistance in nosocomial pathogens: no
711 ESKAPE. *J Infect Dis* **197**:1079–81. doi:10.1086/533452

712 Rumbo-Feal S, Gómez MJ, Gayoso C, Álvarez-Fraga L, Cabral MP, Aransay AM, Rodríguez-
713 Ezpeleta N, Fullaondo A, Valle J, Tomás M, Bou G, Poza M. 2013. Whole Transcriptome
714 Analysis of Acinetobacter baumannii Assessed by RNA-Sequencing Reveals Different mRNA
715 Expression Profiles in Biofilm Compared to Planktonic Cells. *PLoS One* **8**:1–19.
716 doi:10.1371/journal.pone.0072968

717 Russo TA, Manohar A, Beanan JM, Olson R, MacDonald U, Graham J, Umland TC. 2016. The
718 Response Regulator BfmR Is a Potential Drug Target for Acinetobacter baumannii . *mSphere*
719 **1**:1–19. doi:10.1128/msphere.00082-16

720 Sahu PK, Iyer PS, Oak AM, Pardesi KR, Chopade BA. 2012. Characterization of eDNA from the
721 Clinical Strain Acinetobacter baumannii AIIMS 7 and Its Role in Biofilm Formation. *Sci World*
722 *J* **2012**. doi:10.1100/2012/973436

723 Santos-Lopez A, Marshall CW, Scribner MR, Snyder DJ, Cooper VS. 2019. Evolutionary pathways
724 to antibiotic resistance are dependent upon environmental structure and bacterial lifestyle. *Elife*
725 **8**:1–23. doi:10.7554/elife.47612

726 Singh R, Sahore S, Kaur P, Rani A, Ray P. 2016. Penetration barrier contributes to bacterial biofilm-
727 associated resistance against only select antibiotics , and exhibits genus- , strain- and antibiotic-
728 specific differences. *Pathog Dis* 2–7. doi:10.1093/femspd/ftw056

729 Smith MG, Gianoulis T a, Pukatzki S, Mekalanos JJ, Ornston LN, Gerstein M, Snyder M. 2007. New
730 insights into Acinetobacter baumannii pathogenesis revealed by high-density pyrosequencing
731 and transposon mutagenesis. *Genes Dev* **21**:601–14. doi:10.1101/gad.1510307

732 Surgalla MJ, Beesley ED. 1969. Congo red-agar plating medium for detecting pigmentation in
733 Pasteurella pestis. *Appl Microbiol* **18**:834–837.

734 Takajashi A, Yomoda S, Ushijima I, Inoue M. 1995. Orfloxacin, norfloxacin and ceftazimide
735 increase the production of alginate and promote the formation of biofilm of Pseudomonase
736 aeruginosa in vitro. *J Antimicrob Chemother*.

737 Tashjian TF, Lin I, Belt V, Cafarelli TM, Godoy VG. 2017. RNA primer extension hinders DNA
738 synthesis by Escherichia coli mutagenic DNA polymerase IV. *Front Microbiol* **8**:1–9.
739 doi:10.3389/fmicb.2017.00288

740 Tomaras AP, Dorsey CW, Edelmann RE, Actis LA. 2003. Attachment to and biofilm formation on
741 abiotic surfaces by Acinetobacter baumannii: Involvement of a novel chaperone-usher pili
742 assembly system. *Microbiology* **149**:3473–3484. doi:10.1099/mic.0.26541-0

743 Tomaras AP, Flagler MJ, Dorsey CW, Gaddy JA, Actis LA. 2008. Characterization of a two-
744 component regulatory system from Acinetobacter baumannii that controls biofilm formation and

745 cellular morphology. *Microbiology* **154**:3398–3409. doi:10.1099/mic.0.2008/019471-0

746 Vlamakis H, Chai Y, Beauregard P, Losick R, Kolter R. 2013. Sticking together: Building a biofilm
747 the Bacillus subtilis way. *Nat Rev Microbiol* **11**:157–168. doi:10.1038/nrmicro2960

748 Walter BM, Cartman ST, Minton NP, Butala M, Rupnik M. 2015. The SOS Response Master
749 Regulator LexA Is Associated with Sporulation, Motility and Biofilm Formation in Clostridium
750 difficile. *PLoS One* **10**:e0144763. doi:10.1371/journal.pone.0144763

751 Wang N, Ozer EA, Mandel MJ, Hauser AR. 2014. Genome-wide identification of Acinetobacter
752 baumannii genes necessary for persistence in the lung. *MBio* **5**:1–8. doi:10.1128/mBio.01163-14

753 Wang Y, Huang T, Yang Y, Kuo S, Chen C. 2018. Biofilm formation is not associated with worse
754 outcome in Acinetobacter baumannii bacteraemic pneumonia. *Sci Rep* 1–10.
755 doi:10.1038/s41598-018-25661-9

756 Werner E, Roe F, Bugnicourt A, Franklin MJ, Heydorn A, Molin S, Pitts B, Stewart PS. 2004.
757 Stratified Growth in Pseudomonas aeruginosa Biofilms. *Appl Environ Microbiol* **70**:6188–6196.
758 doi:10.1128/AEM.70.10.6188

759 Witkowski TA, Grice AN, Stinnett DB, Wells WK, Peterson MA, Hare JM. 2016. UmuDAb : An
760 Error-Prone Polymerase Accessory Homolog Whose N-Terminal Domain Is Required for
761 Repression of DNA Damage Inducible Gene Expression in Acinetobacter baylyi. *PLoS One* 1–
762 19. doi:10.1371/journal.pone.0152013

763

764

765